J. Ocean Univ. China (Oceanic and Coastal Sea Research)
DOI 10.1007/s11802-013-1870-0
ISSN 1672-5182, 2013 12 (1): 13-22
http://www.ouc.edu.cn/xbywb/
E-mail:xbywb@ouc.edu.cn

Effects of Tidal Currents on Nonlinear Internal Solitary Waves in the South China Sea

FAN Zhisong[1), *], SHI Xingang[2)], Antony K. Liu[3)], LIU Hailong[4)], and LI Peiliang[1)]

1) *College of Physical and Environmental Oceanography*, *Ocean University of China*, *Qingdao* 266100, *P. R. China*
2) *Beijing Branch of CNOOC Energy Technology and Services Limited*, *Beijing* 100027, *P. R. China*
3) *Ocean Sciences Branch*, *NASA Goddard Space Flight Center*, *Greenbelt*, *Maryland*, MD20771, *USA*
4) *State Key Laboratory of Numerical Modeling for Atmospheric Sciences and Geophysical Fluid Dynamics*, *Institute of Atmospheric Physics*, *Chinese Academy of Sciences*, *Beijing* 100029, *P. R. China*

(Received June 10, 2011; revised September 5, 2011; accepted April 16, 2012)
© Ocean University of China, Science Press and Springer-Verlag Berlin Heidelberg 2013

Abstract The propagation and fission process of internal solitary waves (ISWs) with amplitudes of about 170 m are simulated in the northeast of the South China Sea (NSCS) by using the generalized Korteweg-de Vries (KdV) equation under continuous stratification. More attention is paid to the effects of the ebb and flood background currents on the fission process of ISWs. This kind of background current is provided by the composed results simulated in terms of monthly mean baroclinic circulation and barotropic tidal current. It is found that the obtained relation of the number of fission solitons to the water depth and stratification is roughly in accordance with the fission law derived by Djordjevic and Redekopp in 1978; however, there exists obvious difference between the effects of the ebb and flood background currents on the wave-lengths of fission solitons (defined as the distance between two neighboring peaks of ISWs). The difference in nonlinearity coefficient α between the ebb and flood background currents is a main cause for the different wave-lengths of fission solitons.

Key words internal solitary waves; tidal current; fission process; the South China Sea

1 Introduction

Recently, large-amplitude internal solitary waves (ISWs) were observed in the northeast of the South China Sea (NSCS), and in the deep basin of the NSCS the amplitudes of ISWs could reach 170 m (Duda *et al*., 2004; Ramp *et al*., 2004; Yang *et al*., 2004; Lien *et al*., 2005; Klymak *et al*., 2006). So far, the generation mechanism of these waves is not very clear. In Table III of Ramp *et al*. (2004) the two-layer KdV theory produces phase speeds that are too high and produces half-widths that are too small by a factor of two. The two-layer generalized KdV theory returns much better agreement with the observations for both the width and phase speed for waves of moderate amplitudes, but breaks down completely for the very large-amplitude waves (>88 m). The characteristic width of solitons can be determined theoretically from the SAR data based on two-layer KdV-type formulations (Zheng *et al.*, 2001). Liu *et al*. (2004a, Table II) compared the soliton widths in the two packets using the *in situ* and SAR/KdV techniques (Zheng *et al*., 2001). The result was quite good for the first packet (1.4 *versus* 0.9–1.5 km), but much larger based on the SAR data for the second packet (2.5 *versus* 1.4–1.6 km). As pointed out by Ramp *et al*. (2004), there exists a difficulty in simulating large-amplitude ISWs by using the conventional approaches.

Considerable effort has been made to study the assured model of oceanic nonlinear internal waves. It should be pointed out that for broad continental shelves or marginal seas, such as the NSCS, one cannot accomplish simultaneously the simulation of both the generation process of internal tidal waves or ISWs over a steep topographic feature and their long shoreward propagation process by using one model, because there are remarkable differences between the occurrence circumstance and dynamic property of the waves in the former process and those in the latter process. Since 1990's, Lamb and his co-workers have developed a fully-nonlinear non-hydrostatic model (Lamb, 1994; Lamb and Yan, 1996; Lamb, 1997; Warn-Varnas *et al*., 2005, 2010). In this model, Lamb *et al*. consider that strong tidal flow in a stratified fluid over steep topography, and take a specified tidal current with varying strength within a range of choice as the left boundary condition, and an outward current as the right boundary condition. The model can describe meticulously the generation process of internal tide and ISWs over steep topography, and their propagation process near the

* Corresponding author. Tel: 0086-532-66782355
E-mail: fanzhs@hotmail.com

source; however, it is difficult to utilize this model to describe the long shoreward propagation process of these waves on broad continental shelves or in marginal seas. The main reason is that, in the long shoreward propagation process, the internal tide and ISWs undergo the impact of the background currents (the monthly mean baroclinic circulation, the barotropic tidal current, the inertial current, and so on), and this kind of impact cannot be considered by specifying a tidal current on the left boundary and adding a steady background current in the model of Lamb *et al*. (Warn-Varnas *et al*., 2010). Recently, by using the nonhydrostatic Regional Ocean Modeling System, Buijsman *et al*. (2010) performed the modeling of ISWs generated at the Luzon ridge with the model applied in the mixed tidal lee wave regime.

As for the effect of background currents on ISWs, many researchers have done a great many theoretical studies and practical investigations, and achieved some significant results. Grimshaw *et al*. (2002) gave a perfect deduction of higher-order KdV models for ISWs in the absence of rotation. They decompose the horizontal velocity field into the basic component $U(z)$ (background current) and the perturbation. For stable waves, the long wave speeds $c_n^{\pm}$ (n=0, 1, 2, ⋯) corresponding to the modal function $\Phi(z)$ must satisfy $c_n^{+} > U_M = \max U(z)$ and $c_n^{-} < U_m = \min U(z)$. A sufficient condition to exclude any unstable waves is that the Richardson number $R_i = N^2 / U_z^{\,2} > 1/4$. Pelinovskii *et al*. (2000) studied nonlinear internal waves in the ocean stratified in density and current by adopting a two-layer ocean model with a constant background current U_0 in the upper layer and a three-layer ocean model with a constant background current U_0 in the intermediate layer. Gerkema (1996) derived a new two-layer model referred to as the forced rotation-modified Boussinesq equations based on the framework of the KdV and nonlinear Klein-Gordon equations. Zhou and Grimshaw (1989) studied the effect of variable depth-independent currents (geostrophic current, tidal current and inertial current) on ISWs, and obtained a number of analytical expressions concerning the variation in the solitary wave amplitude. Liu (1988) discussed the effects of background shear current on internal wave parameters based on the limited data from moorings in the New York Bight. In the study of the Sulu Sea experiment, Apel *et al*. (1985) adopted the mean axial current (measured at Station SS3 prior to the arrival of each ISW packet) as background shear current in order to determine the coefficients of the KdV equation. Holloway *et al*. (1997) took the averages of measured current and temperature data over 10 d, 4 d and 12 h respectively to investigate the influence of these values on the coefficients of the generalized KdV equation. However, their simulation results indicate that even taking the average over 12 h, the application of the model is not successful in some cases owing to large temporal and spatial variability of the nonlinearity coefficient. However, in the study of the rotation-modified generalized KdV equation model, Holloway *et al*. (1999) did not consider the effects of background currents on the northwest shelf of Australia, perhaps owing to the lack of observed data of background currents. Fan *et al*. (2008a, b) noticed that in a shoreward propagation of internal tide or ISWs over the shelf region in the north of the SCS, these waves undergo a striking contrast of background currents in both current direction and current vertical structure between the ebb tide and flood tide, and the nonlinear coefficients of the generalized KdV equation on the ebb are different from those on the flood. By using the linear modal equations Cai *et al*. (2008) studied the effects of background currents on the internal wave structure. They found that the current shear has little effect on the wave structure, whilst the current curvature could have a strong impact on it.

Lamb *et al*. (Lamb and Yan, 1996; Lamb, 1997) made comparisons between the results by using their fully nonlinear numerical model and those by using the KdV weakly nonlinear theory in the nonlinear evolution of internal waves and in the particle transport by ISWs. Therefore, the fully nonlinear numerical model is significantly superior to the KdV weakly nonlinear theory. However, these comparisons were made without consideration of the effects of background currents.

The generalized KdV model with continuous stratification is a powerful tool for the study of long shoreward propagation process of ISWs. Based on Holloway *et al*. (1997) and Grimshaw *et al*. (2002), we use the generalized KdV model to simulate the propagation and fission process of the ISWs as mentioned earlier with the amplitude of 170m in the deep sea (deep basin and continental slope area) of the NSCS, to explore the propagation and fission mechanism of large-amplitude ISWs. What we are concerned about is the effects of both ebb and flood background current on the fission process of ISWs, the background current being taken from the composed results simulated in terms of monthly mean baroclinic circulation and barotropic tidal current. We find that the obtained relation of the number of fission solitons to the water depth and stratification accords roughly with the fission law derived by Djordjevic and Redekopp (1978); however, we have observed an obvious difference between the effects of the ebb and flood background current on the wave-lengths of fission solitons (defined as the distance between the two neighboring peaks of ISWs). The difference in nonlinearity coefficient α between the ebb and flood background current is a main cause for the different wave-lengths of fission solitons. This study is a contribution to the fission theory of soliton in the existing literature, and benefits understanding the complex propagation and fission process of ISWs in the NSCS.

2 The Generalized KdV Model

In fact the vertical displacement of the isopycnal of ISWs can be expressed in the form $\eta(x,t)\Phi(z)$, where z is a vertical coordinate and positive upward, $\Phi(z)$ is the vertical structure function of vertical-displacement amplitude of an internal wave mode, and $\eta(x,t)$ satisfies the generalized KdV equation with continuous stratification as follows (Holloway *et al*., 1997; Fan *et al*., 2008a):

$$\frac{\partial \eta}{\partial t}+c\frac{\partial \eta}{\partial x}+\alpha\eta\frac{\partial \eta}{\partial x}+\beta\frac{\partial^3 \eta}{\partial x^3}+\frac{c}{2Q}\frac{dQ}{dx}\eta+\frac{\kappa c}{h^2}\eta|\eta|-\nu\frac{\partial^2 \eta}{\partial x^2}=0, \quad (1)$$

where t is time, x is the horizontal coordinate, c is the phase speed of long internal waves, α is the nonlinearity coefficient, β is the dispersion coefficient, $Q(x)$ is a result of slowly varying depth and of horizontal variability in background density and shear flow, κ is the empirical coefficient in the quadratic bottom friction, v is the empirical coefficient of the turbulent horizontal eddy viscosity, and $h=\sqrt{\beta/c}$ represents the vertical scale of the mode of the internal wave.

The vertical structure $\Phi(z)$ is determined by the solution of the eigenvalue problem

$$\frac{\mathrm{d}}{\mathrm{d}z}\left[(c-U)^2\frac{\mathrm{d}\Phi}{\mathrm{d}z}\right]+N^2(z)\Phi=0,\ \Phi(-H)=\Phi(0)=0, \quad (2)$$

where $N(z)$ and $U(z)$ are the Brunt-Väisälä frequency and the background current speed respectively, H is the local depth of water, and the value of $\Phi(z)$ is normalized by its maximal value. Then $\eta(x,t)$ is the isopycnal with maximum displacement.

The coefficients α, β and Q are defined as follows

$$\alpha=\left(\frac{3}{2}\right)\frac{\int_{-H}^{0}(c-U)^2(\mathrm{d}\Phi/\mathrm{d}z)^3\mathrm{d}z}{\int_{-H}^{0}(c-U)(\mathrm{d}\Phi/\mathrm{d}z)^2\mathrm{d}z}, \quad (3)$$

$$\beta=\left(\frac{1}{2}\right)\frac{\int_{-H}^{0}(c-U)^2\Phi^2\mathrm{d}z}{\int_{-H}^{0}(c-U)(\mathrm{d}\Phi/\mathrm{d}z)^2\mathrm{d}z}, \quad (4)$$

$$Q=\frac{c^2\int_{-H}^{0}(c-U)(\mathrm{d}\Phi/\mathrm{d}z)^2\mathrm{d}z}{c_0^2\int_{-H}^{0}(c_0-U_0)(\mathrm{d}\Phi_0/\mathrm{d}z)^2\mathrm{d}z}, \quad (5)$$

where the values with index '0' are the values at any fixed point x_0; it is convenient to use the origin and put x_0=0, usually corresponding to the deepest water station (station S1 in this work, see the next section). The nonlinearity coefficient α and dispersion coefficient β are the coefficients in the well-known KdV equation for ISWs for arbitrary stable vertical stratification and background shear flow; for the deduction of expressions (3) and (4) one may consult Grimshaw *et al*. (2002, Eqs. (63) and (64)). Holloway *et al*. (1997) pointed out that account must be taken of the horizontal variability of the ocean medium, and the KdV equation must be modified. If the horizontal variability is smooth, the reflection of the wave energy from the shelf can be ignored. By using the asymptotic procedure (Pelinovsky *et al*., 1977; Zhou and Grimshaw, 1989), Holloway *et al*. (1997) obtained a modified KdV equation, in which the term $(\frac{c}{2Q}\frac{dQ}{dx}\eta)$ reflecting the effect of slowly varying depth and of horizontal variability in background density and shear flow is added, with Q given in Eq. (5).

After making the following substitutions

$$s=\int_0^x\frac{\mathrm{d}x}{c(x)}-t, \quad (6)$$

$$\xi=\eta\sqrt{Q(x)}. \quad (7)$$

Eq. (1) is reduced to

$$\frac{\partial \xi}{\partial x}+\frac{\alpha}{c^2\sqrt{Q}}\xi\frac{\partial \xi}{\partial s}+\frac{\beta}{c^4}\frac{\partial^3 \xi}{\partial s^3}+\frac{\kappa c}{\beta\sqrt{Q}}\xi|\xi|-\frac{\nu}{c^3}\frac{\partial^2 \xi}{\partial s^2}=0. \quad (8)$$

Eq. (8) is the basic equation used for the simulation of the propagation of ISWs. After the numerical solution of Eq. (8) has been obtained, the vertical displacement $\eta_1(x, s, z)$ of the isopycnal may be written in terms of Eq. (7) at any station (x):

$$\eta_1(x,s,z)=\xi(x,s)\Phi(z)/\sqrt{Q(x)}. \quad (9)$$

By using Eqs. (6) and (9) the vertical velocity $w(x, s, z)$ of the internal wave field may be approximately written as

$$w(x,s,z)=\frac{\partial \eta_1}{\partial t}=\frac{-\Phi(z)}{\sqrt{Q(x)}}\frac{\partial \xi(x,s)}{\partial s}. \quad (10)$$

According to the following stream function (Holloway *et al*., 1999)

$$\Psi(x,t,z)=c\eta(x,t)\Phi(z), \quad (11)$$

the horizontal velocity $u(x, t, z)$ of the internal wave field may be approximately written as

$$u(x,t,z)=c\eta(x,t)\frac{\partial\Phi(z)}{\partial z}. \quad (12)$$

The propagation of an internal wave is accompanied by energy losses due to bottom friction and horizontal diffusion. The bottom turbulent boundary layer is parameterized by the empirical expression for the bottom friction stress in the Chezy form or quadratic bottom friction (Holloway *et al*., 1997):

$$\tau_b=\rho\kappa u|u|, \quad (13)$$

where ρ is the seawater density, u is the near-bottom velocity outside the boundary layer, and κ is the empirical coefficient ($\kappa\sim0.001-0.0026$). The empirical coefficient of the turbulent horizontal eddy viscosity v is a large value in the generalized KdV model. Liu *et al*. (1985) used v=

10–30 $m^2 s^{-1}$ for soliton modeling in the Sulu Sea; in a study of internal waves in the New York Bight, Liu (1988) estimated v to be of the order of 1 $m^2 s^{-1}$; and Sandstrom and Oakey (1995) obtained 0.2 $m^2 s^{-1}$ as an average value of v for the Scotian Shelf.

In this work we chiefly concern ourselves about the effects of background currents on ISWs in the deep water of the NSCS, so the higher-order nonlinear term (the cubic nonlinearity term) may not be significant where there is no critical depth and the nonlinear term is very small or even changes signs. The decay and return effect of rotation on the propagation of ISWs was examined by Helfrich (2007, 2008) using a new rotating extension of a fully nonlinear, weakly nonhydrostatic theory. The nonlinear tide solutions and the disintegration process are briefly explored by Helfrich (2008) for conditions of the northeastern South China Sea. In studing long shoreward propagation process of ISWs from the Luzon Strait to the coastal zone of the NSCS, indeed, the effect of rotation should be considered (Farmer *et al*., 2009). In this paper, to give prominence to the effects of background currents on ISWs, the role of rotation is not considered, which may be a defect.

3 Model Initialization

The climatic data of temperature and salinity in May, the month in which the ISWs under consideration were observed, are downloaded from http://www.nodc.noaa.gov and used to evaluate the Brunt-Väisälä frequency $N(z)$. These data in the world ocean have a resolution of 0.25°× 0.25° grid in the horizontal and 24 layers in the vertical. The required data of 33 layers in the vertical can be obtained by interpolating the downloaded data.

The determination of the background currents $U(z)$ is a difficult problem in the study of propagation and fission process of ISWs. Here we emphasize two points as follows: a) For broad continental shelves or marginal seas the measurements of background currents are expensive. Could we utilize the modeled results of background currents instead of the measured data? A tentative experiment is made in this paper; b) On continental shelf the barotropic tidal current is far greater than the mean baroclinic circulation in general, for example, in the Celtic Sea and in Massachusetts Bay where the generation and fission of internal tides have been considered by Gerkema (1996). However, in the deep water (deep basin and continental slope area) of the NSCS the monthly mean baroclinic circulation is larger than the barotropic tidal current (in absolute value) in the upper layer, as shown in Fig.2 and Table 1 in the following text. Therefore, both barotropic tidal current and monthly mean baroclinic circulation should be taken into account. In this paper we only consider the current composed of the monthly mean baroclinic circulation and barotropic tidal current, which is a simple approximation to determine the background currents $U(z)$. The monthly mean baroclinic circulation is obtained from the results modeled by using the LICOM1.0, which is a quasi-global (65°N–75°S) model and has a resolution of a uniform 0.5°×0.5° grid in the horizontal and 30 layers in the vertical (of the 30 layers 12 are in the upper 300m) (Liu *et al*., 2004b; Liu *et al*., 2005). A 950-year spin-up run was conducted from the initially motionless ocean with its temperature and salinity fields. Then the modeled results are interpolated onto 0.25°× 0.25° grids. The barotropic tidal current is from the results modeled in the SCS (2°–25°N, 99°–122°E,) by using the barotropic POM model without the effect of wind. In modeling the barotropic tide, a 30-d spin-up run was conducted with a horizontal resolution of 1/3°×1/3° grid, the boundary conditions being the same as in the Fes95 model (Le *et al*., 1998), and only the semidiurnal M_2 and S_2, the diurnal K_1 and O_1 are taken into account. The modeled results are given for the surface, middle and bottom layers in according to σ coordinates (the value of σ is 0.0, −0.3, and −1.0 respectively). Because the difference between the three layers is very small, we will adopt the surface result as being representative of barotropic tidal current in the following numerical simulation. By interpolating the values of barotropic tidal current from the 1/3°×1/3° grid to the 0.25°×0.25° grid, we can obtain the background currents $U(z)$.

Observations show that the large-amplitude ISWs propagate westwards along the latitudinal zone of 21°N, 117.5°–118.5°E in May (Klymak *et al*., 2006). Therefore, in the following simulation we consider merely the eastern component U of the background current. The sea floor map and the modeled stations along the latitudinal zone of 21°N are depicted in Fig.1. In addition, the vertical profiles of the U component of the baroclinic circulation at stations S1–S7 in May are shown in Fig.2. A westward background current (about −0.1 $m s^{-1}$) was observed by Klymak *et al*. (2006), which is in accord with the background currents $U(z)$ at station S1 as shown in Fig.2 (at station S1) and Table 1.

Because the barotropic tidal currents in this region are a mixed flow in May (Beardsley *et al*., 2004), we adopt the characteristic value of the barotropic tidal current to perform the diagnostic modeling. The speeds and direc-

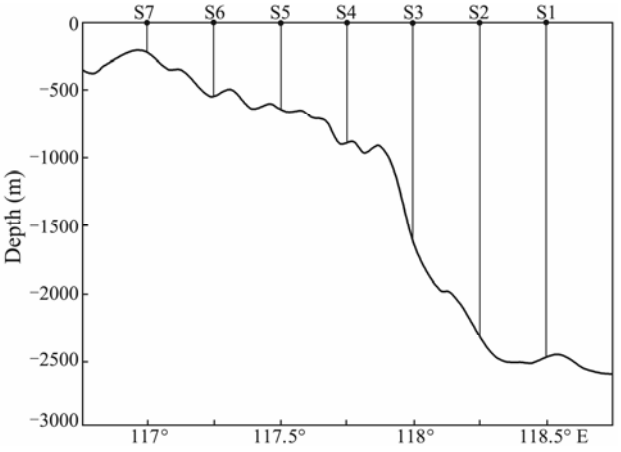

Fig.1 The sea floor map and the modeled stations (S1–S7) along the latitudinal zone of 21°N in the NSCS. The ordinate is depth (m) and the abscissa is geographic longitude.

tions of the barotropic tidal currents at station S7 (situated in the continental slope area) and station S3 (situated in the sea basin area) respectively are listed in Table 1. These values are the results composed of the M_2 and S_2 semidiurnal constituent currents and the K_1 and O_1 diurnal constituent currents at the interval of 1 h. The direction 0° in Table 1 points to the east, and the direction rotates clockwise. Therefore, the characteristic value of the barotropic ebb current is set at 0.04 m s^{-1} (eastward) and that of the flood current at 0.02 m s^{-1} (westward) as shown in Table 1.

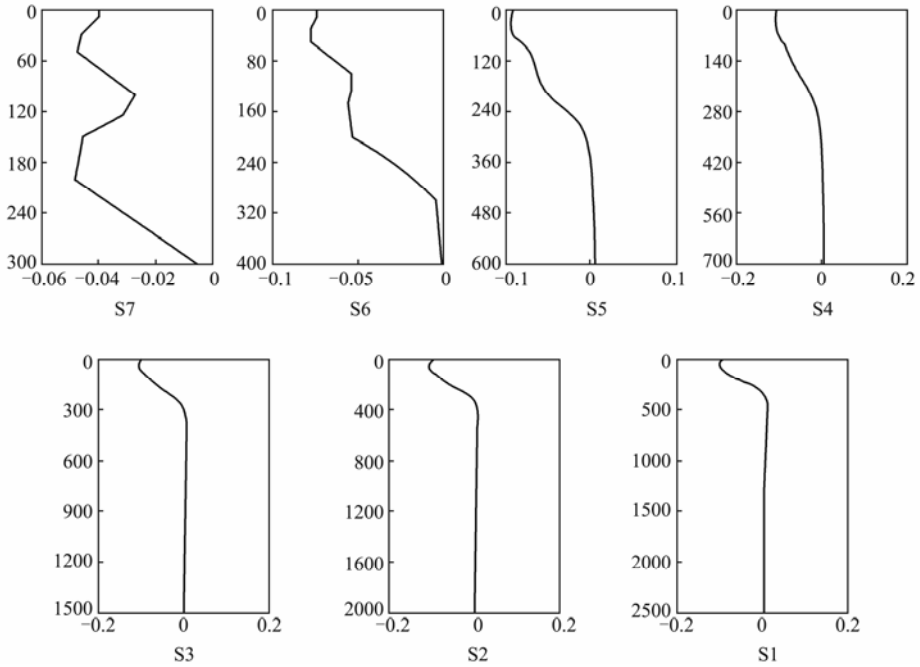

Fig.2 The vertical profiles of the *U* component of the monthly mean baroclinic circulation at stations S1–S7 in May obtained from the results modeled by using the LICOM1.0 (Liu *et al*., 2004b; Liu *et al*., 2005). The ordinate is depth (m) and the abscissa is velocity (m s^{-1}).

Table 1 The speeds and directions of barotropic tidal currents at stations S7 and S3

Time sequence	S7		S3	
	V (m s^{-1})	Direction (°)	V (m s^{-1})	Direction (°)
0	0.032	18.43	0.03	0
1	0.022	26.57	0.032	18.43
2	0.014	45.0	0.022	26.57
3	0.01	90	0.014	45.0
4	0.01	90	0.01	90
5	0.01	−180	0	0
6	0.01	−180	0	0
7	0.02	−180	0.01	−180
8	0.02	−180	0.014	−135
9	0.02	−180	0.014	−135
10	0.02	−180	0.014	−135
11	0.02	−180	0.01	−90
12	0.01	−180	0.01	−90
13	0.01	−180	0.01	−90
14	0.02	−180	0	0
15	0.02	−180	0.01	−180
16	0.02	−180	0.01	−180
17	0.022	153.43	0.01	−180
18	0.014	135	0	0
19	0.01	90	0	0
20	0.01	90	0	0
21	0.022	26.57	0.01	0
22	0.032	18.43	0.02	0
23	0.041	14.04	0.032	18.43
24	0.041	14.04	0.041	14.04

In the following diagnostic modeling, the assumption of westwards propagation of the initial soliton on both the ebb and flood is only an approximation. In fact, between stations S7 and S1 the barotropic tidal current is temporally variable at every station. However, we note that the impact of barotropic tidal current on the composed background currents $U(z)$ mainly occurs during the travel of ISWs from station S4 to station S7, because the monthly mean baroclinic circulation diminishes gradually in the shoaling continental slope area (Fig.2). The distance between stations S4 and S7 is about 75 km. On the ebb, the average of the soliton velocity V over this distance is 1.94 m s^{-1}, and the travel time of ISWs from station S4 to station S7 is about 10.74 h. Because the diurnal barotropic tidal current is dominant in this sea area (Zhao and Alford, 2006), we utilize this fact as a preliminary procedure.

At sations S1-S7 the vertical structure function $\Phi(z)$ of vertical-displacement amplitude and the phase speed c of long internal waves for a mode are calculated with Eq. (2) by using the numerical calculation method of eigenvalue problem (2), which is developed on the basis of Thompson-Haskell's calculation method (Shi *et al*., 2009); then the coefficients α, β and Q of the generalized KdV equation can be calculated with Eqs. (3)–(5). The profiles of the density and the Brunt-Väisälä frequency $N(z)$ at stations S1 and S7 are depicted in Figs.3 and 4 respectively. The vertical profiles of $\Phi(z)$ for the first, second and third modes at stations S1 and S7 are shown in Fig.5. In this figure

and the following figures (Figs.5–10), the solid curve and dashed curve represent results on the ebb and flood, respectively. The distributions of c, α, β and Q corresponding to the first mode are shown in Figs.6–9, respectively.

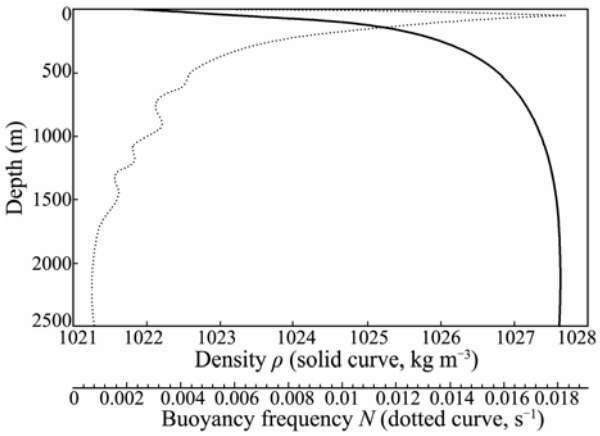

Fig.3 The vertical profiles of the density (solid curve) and the Brunt-Väisälä frequency $N(z)$ (dashed curve) at station S1 calculated from the climatic data of temperature and salinity in May downloaded from http://www.nodc.noaa.gov.

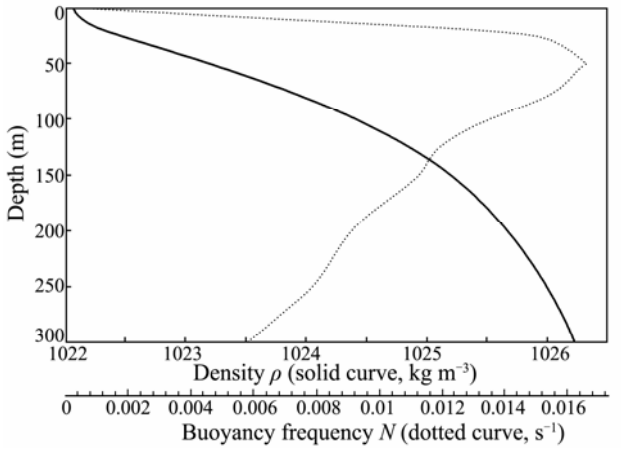

Fig.4 As in Fig.3 but at station S7.

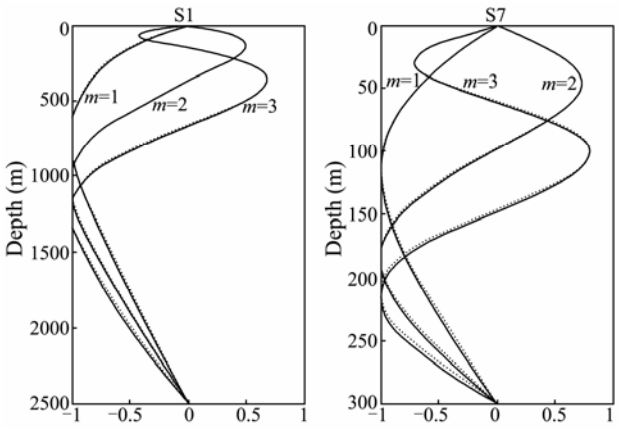

Fig.5 The vertical profiles of $\Phi(z)$ for the first, second and third modes at stations S1 (left) and S7 (right). The solid and dashed curves represent results on the ebb and flood, respectively.

It is evident in Fig.5 that the total difference of effect between the ebb and flood background current on the vertical modal structure is small for the first mode, but for the second and third modes, the influence in the continental slope area is slightly bigger than that in the sea basin area. In fact, at station S1 the maximal differences between $\Phi(z)$ on the ebb and the flood for the first, second and third modes are 0.011, 0.014, and 0.025 respectively. Moreover, at station S7 the corresponding maximal differences are 0.015, 0.043, and 0.069 respectively. Fig.6

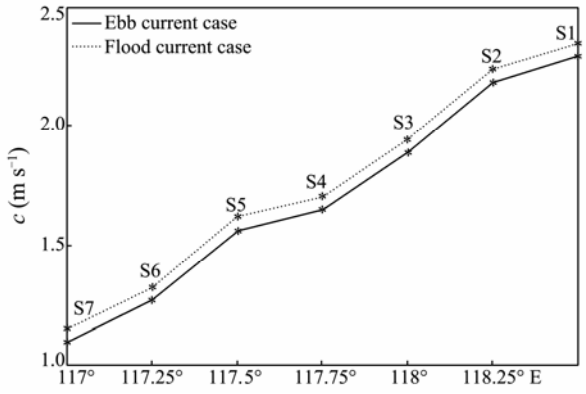

Fig.6 The phase speed c of long internal waves between stations S1–S7 corresponding to the first mode. The solid and dashed curve represent results on the ebb and flood, respectively.

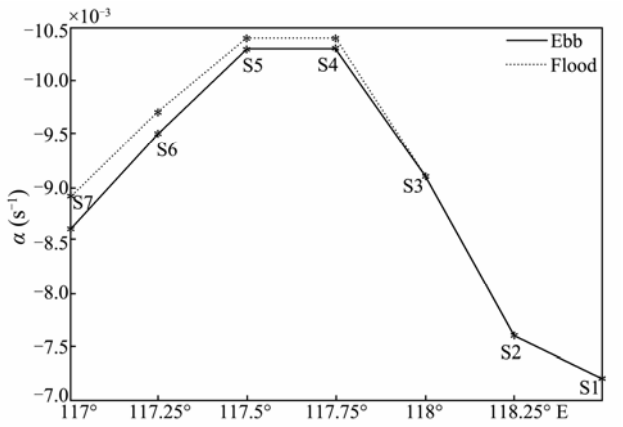

Fig.7 As in Fig.6 but for the nonlinearity coefficient α.

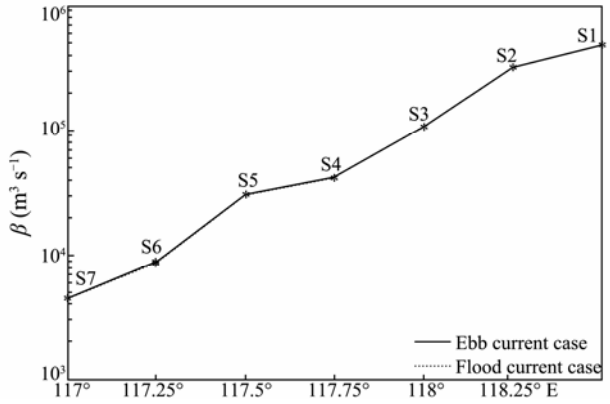

Fig.8 As in Fig.6 but for the dispersion coefficient β.

shows clearly that the phase speed c of long internal waves on the flood is larger than that on the ebb. As shown in Fig.2, at stations S1–S7, the direction of the U component of baroclinic circulation in May is westward; this is the same direction as that of the barotropic tidal current on the flood, so the composed background currents $U(z)$ on the flood is larger than that on the ebb. The larger c on the flood might be due to the larger advection of the flood background currents. It can be seen from Fig.7 that there is a distinct difference between the effects of the ebb and flood background current on α at stations S4–S7 (in the continental slope area), and this difference becomes larger with shoaling, and that the absolute value of α is always larger on the flood. However, Figs.8 and 9 indicate that the effects of the ebb and flood background currents on β (or Q) almost have no difference.

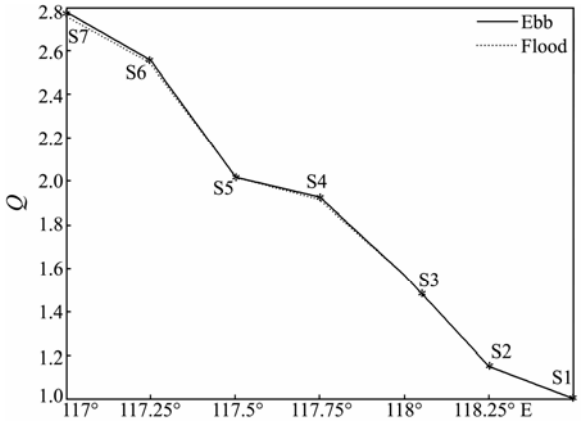

Fig.9 As in Fig.6 but for the horizontal variability coefficient Q.

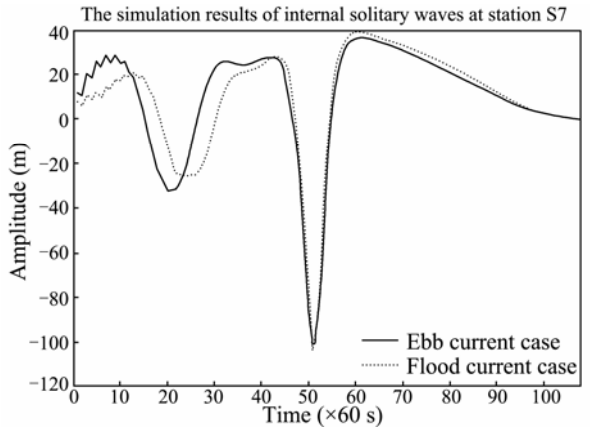

Fig.10 The ISWs arriving at station S7.

4 Nonlinear Fission of Large-Amplitude ISWs

The finite difference form of Eq. (8) is (Holloway *et al*., 1997)

$$\frac{\xi_j^{n+1}-\xi_j^{n-1}}{D}+\frac{\alpha_i}{c_i^2\sqrt{Q_i}}\frac{\xi_{j+1}^n-\xi_{j-1}^n}{T}+$$

$$\frac{\beta_i}{c_i^2}\frac{\xi_{j+2}^n-2\xi_{j+1}^n+2\xi_{j-1}^n-\xi_{j-2}^n}{T^3}+\frac{2\kappa c_i}{\beta_i\sqrt{Q_i}}\xi_j^n\left|\xi_j^n\right|-$$

$$\frac{2\nu}{c_i^3}\frac{\xi_{j+1}^n-2\xi_j^n+\xi_{j-1}^n}{T^2}=0\,, \tag{14}$$

where j, n and i are the suffixes indicating time, space and station respectively, T is the time step length, and D is the horizontal space step length. Because the considered water region is broad, and the water depth shows dramatic variations, the simulation is performed in two sections. At stations S1–S4, κ=0.001 and ν=5.0 $m^2 s^{-1}$ are adopted; at stations S5–S7, κ=0.002 and ν=5.0 $m^2 s^{-1}$ are adopted. Since at stations S5–S7 the bottom friction stress increases because of shoaling, a bigger value of the empirical coefficient κ is adopted. The numerical stability criterion for Eg. (14) with the small values of T is (Holloway *et al*., 1997)

$$D<0.38T^3/\beta\,. \tag{15}$$

A variable horizontal space step length and a fixed time step length (60s) are adopted in using (15). For the first step the difference $(\xi_j^{n+1}-\xi_j^{n-1})/D$ is replaced by $(\xi_j^1-\xi_j^0)/D$, where ξ_j^0 is the value for the initial wave form. The expression of the initial wave form is

$$\xi(s,x=0)=-\xi_0\sqrt{Q(x=0)}\sec h^2\left(\frac{x-Vt}{\Delta}\right), \tag{16}$$

where the expression of the soliton velocity V is

$$V=c+\frac{\alpha\xi_0}{3}\,; \tag{17}$$

the characteristic half width Δ of the soliton is defined as

$$\Delta=\left(\frac{12\beta}{\alpha\xi_0}\right)^{1/2}, \tag{18}$$

and ξ_0 is the amplitude of the initial wave form at station S1. It is noticed that c, α and β are determined by Eqs. (2), (3) and (4), respectively.

In the deep central basin of the SCS (20–21°N, 119°00′–120°40′E), Klymak *et al*. (2006) observed that the prototypical solitons have amplitudes estimated at 170 m, half widths of 3km, and phase speeds of 2.9±0.1 $m\,s^{-1}$. Consulting the observations and in terms of the results of c, α and β calculated previously, we assume that the initial soliton at station S1 has an amplitude ξ_0 of 170 m at the depth of the maximum of $\Phi(z)$ for the first mode (the depth is about 746 m and the density is about 1027.26 $kg\,m^{-3}$, see Fig.5), the values of V and Δ of the initial soliton on the ebb are 2.70 $m\,s^{-1}$ and 3.78 km, respectively, and those on the flood are 2.76 $m\,s^{-1}$ and 3.77 km, respectively. It should be pointed out that the initial wave form Eq. (16) and the above parameters of the initial solitons are only an approximation of the leading soliton observed by Klymak *et al*. (2006). This approximation is suitable

for the goal of this study, which is to explore the propagation and fission mechanism of large-amplitude ISWs. However, to achieve a comprehensive comparison between the modeling results and observations at station S7, the measured data at station S1 must be utilized, because at station S1 the waves are nonlinear internal wave trains evolving from the Luzon Strait (Klymak *et al*., 2006; Farmer *et al*., 2009).

Fig.10 depicts the ISWs arriving at station S7. Assume the westwards propagation of the initial soliton at station S1 is on the ebb as well as on the flood,. At station S7 the solid and dashed curve represent results on the ebb and on the flood, respectively. At station S7 the amplitude of the leading soliton is about 133.95 m at the depth of the maximum of $\Phi(z)$ for the first mode (the depth is about 116 m, and the density is about 1024.70 kg m^{-3}, see Fig.5). The wave-length of ISWs between the leading soliton and the second soliton shown in Fig.10 (defined as the distance between the two peaks of ISWs) is 2.94 km on the ebb, and 2.56 km on the flood. In this figure, to compare the two results on the flood and ebb, we shift the curve to superpose the two leading solitons. In fact, the leading soliton on the flood travels fast, because the phase speed c on the flood is larger than that on the ebb, as shown in Fig.6. In fact, at station S7 the phase speed c is 1.15 m s^{-1} for the first mode on the flood, and 1.09 m s^{-1} on the ebb.

Assume the westwards propagation of the initial solitons at station S1 is on the ebb and on the flood. At station S7 the arrived ISWs are depicted in Fig.10, the amplitude of the leading soliton is about 133.95 m at the depth of the maximum of $\Phi(z)$ for the first mode (the depth is about 116 m, and the density is about 1024.70 kg m^{-3}, see Fig.5). This result and the modeling result of the phase speed c at station S7 (see Fig.6, at station S7 the phase speed c is 1.15 m s^{-1} for the first mode on the flood, and 1.09 m s^{-1} on the ebb) are within the scope of the observed results during ASIAEX at the sea area nearby this station. For example, Ramp *et al.* (2004, Table III) observed that the amplitude and phase speed of large wave are η=142 m, c=1.23 m s^{-1} on May 9, 2001, and η=135 m, c=1.26 m s^{-1} on May 8, 2001. In addition, these modeling results are in accordance with the observed characteristics of large waves by Lien *et al.* (2005) at mooring IW1 close to station S7 in this study. In April 2000, they observed that the leading waves had a vertical displacement of 70–120 m and a wave period of 10–20 min corresponding to a 1–2-km width.

As shown in Fig.10, although the difference between the effects of the ebb and flood background currents on the amplitude and shape of the leading soliton is small, this difference in the nonlinear fission process of ISWs is quite evident.

Nonlinear fission process of ISWs due to variable bottom topography only has been discussed by many researchers, for instance, Djordjevic and Redekopp (1978). They obtained an exact fission law, that is, the relation of the number of fission solitons with the eigendepth and density stratification (Djordjevic and Redekopp, 1978, Eq. (2.19)); it has the form

$$M(M+1)/2=\frac{1}{d_s^{3/2}}\left[\frac{1+\left(\frac{B}{2m\pi}\right)^2}{1+\left(\frac{Bd_s}{2m\pi}\right)^2}\right]^{3/4}\times \frac{1+\left(\frac{Bd_s}{6m\pi}\right)^2}{1+\left(\frac{B}{6m\pi}\right)^2}\frac{(-1)^m-e^{-Bd_s/2}}{(-1)^m-e^{-B/2}}, \quad (19)$$

where M is the number of fission solitons, B is the density distribution coefficient (Djordjevic and Redekopp choose the ambient density distribution $\rho_s(z)=\exp(-Bz)$), (m=1, 2, 3, ⋯) expresses the mode number of internal waves, and d_s is the eigendepth. Djordjevic and Redekopp (1978) discussed the propagation of long internal waves over two-dimensional topography, where the water depth changes rapidly from the deep water depth d_0 to the shallow water depth d_s. And after all lengths are scaled with the depth d_0, then d_0=1 and the eigendepth d_s<1. Using the exact fission law Eq. (19) Djordjevic and Redekopp obtained the fission data in Table 2 for a continuous stratification model.

Table 2 Fission data for a continuous stratification model using the exact law Eq. (19) (Djordjevic and Redekopp, 1978)

B	m	M	d_s
0.005	1	2	0.4809
0.01	1	2	0.4812
0.05	1	2	0.4828
0.1	1	2	0.4849
0.25	1	2	0.4909
0.005	2	2	0.1114
0.01	2	2	0.1116
0.05	2	2	0.1136
0.1	2	2	0.1161
0.25	2	2	0.1239
0.05	3	2	0.4828

In this work, the obtained relation of the number of fission solitons is roughly in accordance with the fission law of Djordjevic and Redekopp (1978). As shown in Figs.1 and 10, for the first mode the eigendepth is about 0.4 (if we assume roughly the typical depth 1000 m for the continental slope area and the typical depth 2500 m for the sea basin), and the number of fission solitons is 2. In addition, our results reveal that background currents have important influence on the wave-length of fission solitons, and the difference between the effects of the ebb and flood background currents on the wave-length is obvious. The difference in nonlinearity coefficient α between the ebb and flood background currents is a main cause for the different wave-lengths of fission solitons. In fact, in this sea area the composed background currents $U(z)$ are always westwards in the upper layer, because the monthly mean baroclinic circulation is larger than the barotropic tidal current (in absolute value) in the upper layer, as

shown in Fig.2 and Table 1. Therefore the initial soliton is traveling westwards in the same direction as are the composed background currents $U(z)$, even if during the ebb background current. The instance of soliton traveling against background current cannot exist in this study. This situation is quite unlike that considered by Gerkema (1996). As shown in Fig.7 the absolute value of α on the flood is always larger than that on the ebb. The stronger nonlinearity on the flood could produce two forms of impact on the propagation and fission process of ISWs as follows:

A) The amplitude of the leading soliton on the flood is a little larger than that on the ebb, as shown in Fig.10;

B) After the leading soliton passes station S7, owing to the more strong nonlinearity, the fission process of the wave on the flood experiences less spatial distance than that on the ebb for the second soliton to arise, as shown in Fig.10. In this figure, to compare the two results on the flood and ebb, we shift one curve to superpose the two leading solitons. In fact, the leading soliton on the flood travels faster, because the phase speed c on the flood is larger than that on the ebb, as shown in Fig.6. In fact, at station S7 the phase speed c is $1.15\,\mathrm{m\,s^{-1}}$ for the first mode on the flood, and $1.09\,\mathrm{m\,s^{-1}}$ on the ebb.

However, this study is only preliminary, leaving some defects and problems to be overcome in further modeling. In the actual long propagation process of internal tide and ISWs the barotropic tidal current is temporally variable at every station. Also, from the analysis of the measured data Klymak *et al*. (2006) pointed out that in the deep central basin of the NSCS the prototypical solitons pass through the pre-existing shear from the inertial wave field, and they may trigger short bursts of dissipation. However, the inertial shear current is not taken into account in the background shear current in this paper owing to the difficulty of modeling it. In addition, in this paper the monthly mean baroclinic circulation reflects only a basic situation in the NSCS. Owing to the monsoon current in the SCS and the Kuroshio water intruding into the SCS and the coastal current in the NSCS (Xue *et al*., 2001; Chapman *et al*., 2004), the variation of baroclinic circulation is significant and complicated in the NSCS. The three-layer stratification of the water column occasionally appearing in the northeast of Tung-Sha Island (Yang *et al*., 2004, 2009) may be due to the common interaction of the 3 current systems, and might be the cause of the two-mode structure of internal waves. For a comprehensive comparison between modeling results and observations, the measured data at the initial station S1 must be utilized, because in this sea area the waves are nonlinear internal wave trains evolving from the Luzon Strait.

5 Summary

In this paper, we study the effects of the ebb and flood background currents on the propagation and fission process of large-amplitude ISWs in the NSCS by using the generalized KdV model. This type of background current was obtained from the composed results simulated in terms of monthly mean baroclinic circulation and barotropic tidal current. We found that the obtained relation of the number of fission solitons to the water depth and stratification is roughly in accordance with the fission law derived by Djordjevic and Redekopp (1978). However, obvious difference exists between the effects of the ebb and flood background currents on the wave-lengths of fission solitons. Moreover, the difference in nonlinearity coefficient α between the ebb and flood background currents is a main cause for the different wave-lengths of fission solitons. It may be of help to study in the future the dynamic process of the long shoreward propagation of large-amplitude ISWs with these results.

Acknowledgements

This work is supported by the Key Program of National Natural Science Foundation of China under contract No. 41030855.

References

Apel, J. R., Holbrook, J. R., Liu, A. K., and Tsai, J. J., 1985. The Sulu Sea internal soliton experiment. *Journal of Physical Oceanography*, **15**: 1625-1651.

Beardsley, R. C., Duda, T. F., Lynch, J. F., Irish, J. D., Ramp, S. R., Chiu, C.-S., Tang, T.-Y., Yang, Y.-J., and Fang, G.-H., 2004. Barotropic tide in the Northeast South China Sea. *IEEE Journal of Oceanic Engineering*, **29** (4): 1075-1086.

Buijsman, M. C., Kanarska, Y., and McWilliams, J. C., 2010. On the generation and evolution of nonlinear internal waves in the South China Sea. *Journal of Geophysical Research*, **115**, C02012, DOI: 10.1029/2009JC005275.

Cai, S., Long, X., Dong, D., and Wang, S., 2008. Background current affects the internal wave structure of the northern South China Sea. *Progress in Natural Science*, **18** (5): 585-589.

Chapman, D. C., Ko, D.-S., and Preller, R. H., 2004. A high-resolution numerical modeling study of the subtidal circulation in the Northern South China Sea. *IEEE Journal of Oceanic Engineering*, **29** (4): 1087-1104.

Djordjevic, V. D., and Redekopp, L. G., 1978. The fission and disintegration of internal solitary waves moving over two-dimensional topography. *Journal of Physical Oceanography*, **8**: 1016-1024.

Duda, T. F., Lynch, J. F., Irish, J. D., Beardsley, R. C., Ramp, S. R., Chiu, C.-S., Tang, T.-Y., and Yang, Y.-J., 2004. Internal tide and nonlinear internal wave behavior at the continental slope in the Northern South China Sea. *IEEE Journal of Oceanic Engineering*, **29** (4): 1105-1130.

Farmer, D., Li, Q., and Park, J.-H., 2009. Internal wave observations in the South China Sea: the role of rotation and non-linearity. *Atmosphere-Ocean*, **47** (4): 267-280.

Fan, Z. S., Zhang, Y. L., and Song, M., 2008a. A study of SAR remote sensing of internal solitary waves in the north of the South China Sea: I. Simulation of internal tide transformation. *Acta Oceanologica Sinica*, **27** (4): 39-56.

Fan, Z. S., Zhang, Y. L., and Song, M., 2008b. A study of SAR remote sensing of internal solitary waves in the north of the South China Sea: II. Simulation of SAR signatures of internal solitary waves. *Acta Oceanologica Sinica*, **27** (5): 36-48.

Gerkema, T., 1996. A unified model for the generation and fis-

sion of internal tides in a rotating ocean. *Journal of Marine Research*, **54**: 421-450.

Grimshaw, R., Pelinovsky, E., and Poloukhina, O., 2002. Higher-order Korteweg-de Vries models for internal solitary waves in a stratified shear flow with a free surface. *Nonlinear Processes in Geophysics*, **9**: 221-235.

Helfrich, K. R., 2007. Decay and return of internal solitary waves with rotation. *Physics of Fluids*, **19**, 02661, DOI: 10.1063/1.2472509.

Helfrich, K. R., 2008. Continuously stratified nonlinear low-mode internal tides. *Journal of Marine Research*, **66** (3): 299-323.

Holloway, P. E., Pelinovsky, E., Talipova, T., and Barnes, B., 1997. A nonlinear model of internal tide transformation on the Australian North West Shelf. *Journal of Physical Oceanography*, **27**: 871-896.

Holloway, P. E., Pelinovsky, E., and Talipova, T., 1999. A generalized Korteweg-de Vries model of internal tide transformation in the coastal zone. *Journal of Geophysical Research*, **104**: 18333-18350.

Klymak, J. M., Pinkel, R., Liu, C.-T., Liu, A. K., and David, L., 2006. Prototypical solitions in the South China Sea. *Geophysical Research Lettters*, **33**, L11607, DOI: 10.1029/2006GL025932.

Lamb, K. G., 1994. Numerical experiments of internal wave generation by strong tidal flow across a finite amplitude bank edge. *Journal of Geophysical Research*, **99** (C1): 843-864.

Lamb, K. G., and Yan, L., 1996. The evolution of internal wave undular bores: comparisons of a fully nonlinear numerical model with weakly nonlinear theory. *Journal of Physical Oceanography*, **26**: 2712-2734.

Lamb, K. G., 1997. Particle transport by nonbreaking, solitary internal waves. *Journal of Geophysical Research*, **102** (C8): 18641-18660.

Le, P., Lyard, F., Molines, J. M., Genco, M. L., and Rabilloud, F., 1998. A hydrodynamic ocean tide model improved by assimilating a satellite altimeter-drived data set. *Journal of Geophysical Research*, **103** (C3): 5513-5529.

Lien, R.-C., Tang, T.-Y., Chang, M.-H., and D'Asaro, E. A., 2005. Energy of nonlinear internal waves in the South China Sea. *Geophysical Research Lettters*, **32**, L05615, DOI: 10.1029/2004GL022012.

Liu, A. K., 1988. Analysis of nonlinear internal waves in the New York Bight. *Journal of Geophysical Research*, **93** (C10): 12317-12329.

Liu, A. K., Holbrook, J. R., and Apel, J. R., 1985. Nonlinear internal wave evolution in the Sulu Sea. *Journal of Physical Oceanography*, **15**: 1613-1624.

Liu, A. K., Ramp, S. R., Zhao, Y., and Tang, T.-Y., 2004a. A case study of internal solitary wave propagation during ASIAEX 2001. *IEEE Journal of Oceanic Engineering*, **29** (4): 1144-1156.

Liu, H. L., Yu, Y. Q., Li, W., and Zhang, X. H., 2004b. *Reference Manual for LASG/IAP Climate System Ocean Model (LICOM1.0)*. Science Press, Beijing, 107pp (in Chinese).

Liu, H. L., Li, W., and Zhang, X. H., 2005. Climatology and variability of the Indonesian Throughflow in the eddy-permitting oceanic GCM. *Advances in Atmospheric Sciences*, **22** (4): 496-508.

Pelinovsky, E., Shavratsky, S., and Raevsky, M. A., 1977. The Korteweg-de Vries equation for nonstationary internal waves in an inhomogeneous ocean. *Izvestiya*, *Atmospheric and Oceanic Physics*, **13**: 373-376.

Pelinovskii, E. N., Polukhina, O. E., and Lamb, K., 2000. Nonlinear internal waves in the ocean stratified in density and current. *Oceanology*, **40** (6): 757-766.

Ramp, S. R., Tang, D., Duda, T. F., Lynch, J. F., Liu, A. K., Chiu, C.-S., Bahr, F., Kim, H. R., and Yang, Y.-J., 2004. Internal solitons in the northeast South China Sea part I: Sources and deep water propagation. *IEEE Journal of Oceanic Engineering*, **29** (4): 1157-1181.

Sandstrom, H., and Oakey, N. S., 1995. Dissipation in internal tides and solitary waves. *Journal of Physical Oceanography*, **25**: 604-614.

Shi, X. G., Fan, Z. S., and Liu, H. L., 2009. A numerical calculation method of eigenvalue problem of nonlinear internal waves. *Journal of Hydrodynamics Ser. B*, **21** (3): 373-378.

Warn-Varnas, A. C., Chin-Bing, S. A., King, D. B., Hawkins, J. A., Lamb, K. G., and Teixeira, M., 2005. Yellow Sea oceanic-acoustic solitary wave modeling studies. *Journal of Geophysical Research*, **110**, C08001, DOI: 10.1029/2004JC002801.

Warn-Varnas, A. C., Hawkins, J., Lamb, K. G., Piacsek, S., Chin-Bing, S., King, D., and Burgos, G., 2010. Solitary wave generation dynamics at Luzon Strait. *Ocean Modelling*, **31** (1-2): 9-27.

Xue, H. J., Chai, F., Xu, J. P., *et al.*, 2001. *The Study of A Circulation Model and Characteristics of Meso-Scale Eddies in the South China Sea. Oceanography in China (13)*. China Ocean Press, Beijing, China. 254pp (in Chinese).

Yang, Y.-J., Tang, T.-Y., Chang, M.-H., Liu, A. K., Hsu, M.-K., and Ramp, S. R., 2004. Solitons northeast of TungSha Island during the ASIAEX pilot studies. *IEEE Journal of Oceanic Engineering*, **29** (4): 1182-1199.

Yang, Y.-J., Fang, Y.-C., Chang, M.-H., Ramp, S. R., Kao, C.-C., and Tang, T.-Y., 2009. Observations of second baroclinic mode internal solitary waves on the continental slope of the northern South China Sea. *Journal of Geophysical Research*, **114**, C10003, DOI: 10.1029/2009JC005318.

Zhao, Z., and Alford, M. H., 2006. Source and propagation of internal solitary waves in the northeastern South China Sea. *Journal of Geophysical Research*, **111**, C11012, DOI: 10.1029/2006JC003644.

Zheng, Q., Yuan, Y., Klemas, V., and Yan, X.-H., 2001. Theoretical expression for an ocean internal soliton synthetic aperture radar image and determination of the soliton characteristic width. *Journal of Geophysical Research*, **106** (C11): 31415-31423.

Zhou, X., and Grimshaw, R., 1989. The effect of variable currents on internal solitary waves. *Dynamics of Atmospheres and Oceans*, **14**: 17-39.

(Edited by Xie Jun)